Single-molecule dynamics of semiflexible Gaussian chains

Shilong Yang, James B. Witkoskie, and Jianshu Cao[a)]
Department of Chemistry, Massachusetts Institute of Technology, Cambridge, Massachusetts 02139

(Received 14 February 2002; accepted 18 September 2002)

A semiflexible Gaussian chain model is used to determine the statistics and correlations of single-molecule fluorescence resonant energy transfer (FRET) experiments on biological polymers. The model incorporates a persistence length in a Rouse chain and describes single-chain dynamics with normal modes. The hydrodynamic interaction is included in the dynamics of the semiflexible Gaussian chain on the preaveraging level. The distribution functions of the fluorescence lifetime and the FRET efficiency provide direct measures of the chain stiffness, and their correlation functions probe the intrachain dynamics at the single-molecule level. When measured with finite time resolution, the instantaneous diffusion coefficient for FRET is much smaller in the collapsed structure than in the coiled structure, and the variation has a quadratic dependence on the donor–acceptor distance. In the fast reaction limit, single-molecule FRET lifetime measurements can be used to map out the equilibrium distribution function of interfluorophore distance. As an example of microrheology, the intrinsic viscoelasticity can be extracted from single-molecule tracking of the Brownian dynamics of polymers in solution. © *2002 American Institute of Physics.*
[DOI: 10.1063/1.1521156]

I. INTRODUCTION

Single-molecule techniques provide a powerful method to measure the conformational structure and dynamics of synthetic and biological polymers. Examples include recent progress in studying the response of single DNA molecules under twisting and stretching and probing the relaxation dynamics of polymers on short time and length scales. One promising candidate for studying these time and length scales in polymers is fluorescence resonant energy transfer spectroscopy (FRET). In these experiments donor and acceptor dye molecules are attached to the polymer at two different points. A laser is used to pump the donor dye to an excited state. Depending on the distance between the donor and acceptor molecule, nonradiative energy transfer from the excited donor dye to the acceptor dye may occur, which results in the fluorescence of the acceptor dye molecule. The light intensity at the fluorescence frequency of the acceptor molecule is strongly dependent on the distance between the two molecules and can be used as a measurement of this distance. With current synthetic techniques, the position of the donor and acceptor dyes on a polymer like DNA can be controlled, which allows us to explore the polymer dynamics on any length scale.[1–14] This technique has been used to investigate the denaturation of chymotrypsin inhibitor, the dynamics and folding of single peptides, the fluorescence lifetime distribution of single TMR molecules, etc.[12,15] A similar technique based on the distance dependence of the electron transfer rate has recently been developed by the Xie group.[2] Using a different set of single-molecule techniques, Chu and co-workers observed the single polymer dynamics in steady shear flow, the relaxation of a single DNA molecule, the response of a flexible polymer to a sudden elongation flow, etc.[16–18] In comparison with bulk experiments, these single-molecule experiments have several advantages, such as the removal of inhomogeneous averaging, the direct observation of intramolecular dynamics without the subtraction of the solvent background as is done in bulk measurements, and site-specific measurement of a polymer chain.[8] Motivated by the experimental progress, we analyze the information revealed by single-molecule measurements and calculate their single-molecule quantities based on the Brownian dynamics of semiflexible ideal Gaussian chains.

An ideal polymer assumes random coil configurations and follows Gaussian chain statistics. Without the explicit consideration of the excluded volume effect and the geometrical constraints, the simple Rouse model treats the connectivity between next neighbor pairs by harmonic bonds. But biological polymers are stiff on the length scale ranging from 5 nm for microtubes, 17 nm for actin, and up to 50 nm for DNA.[13,14] Most single-molecule experiments are performed on length scales where the polymer exhibits some rigidity so that the Rouse Gaussian chain model will have to be extended. In Sec. II, we modify the Gaussian chain model by introducing the persistence length that prevents the polymer from being flexible on all length scales. Similar models for semiflexible chain have been studied by Kratky and Porod, Harris and Hearse, Freed, Fixman and Kovac, Ha and Thirumalai, and others.[19–27] Interest in these semiflexible chain models is revived by the effort to model single-molecule force measurements of proteins and DNAs. Our emphasis here is to formulate the semiflexible model using the analog to the Ornstein–Uhlenbeck random walk process and thus incorporate the persistence length into the Rouse model in a natural and rigorous way.

In order to interpret single-molecule experiments and extract the desired information on polymers, we need to calculate the dynamics of semiflexible chains. In Sec. III, we

[a)]Electronic mail: jianshu@mit.edu

solve the Brownian dynamics by performing a normal mode decomposition of the Langevin equation of a polymer chain. This normal mode decomposition is similar to the standard decomposition performed in the Rouse and Zimm models, with a modification to account for the short length scales that this paper considers. The model calculation can be elaborated by including excluded volume and hydrodynamic effects under a similar approximation made in the Zimm model.[28,29] Using the normal mode approach, we calculate distance–distance correlation functions that are relevant for single-molecule measurements.

In FRET experiments, people can measure the separation of two dye molecules attached to the polymer chain. The fluorescence energy transfer reaction usually occurs on a nanosecond time scale while the intrachain relaxation takes millisecond or even longer.[9,11,12] Hence the FRET lifetime as well as the FRET efficiency is a ''snapshot'' of the transient configuration. The correlations of the FRET lifetime and the FRET efficiency reveal the slow intrachain relaxation process that modifies the donor–acceptor distance. In Sec. IV A, the distribution of E is derived to show different features to distinguish collapsed and coiled conformations. In Secs. IV A and IV B, the FRET efficiency and the lifetime correlation functions are formulated for the semiflexible chain model introduced in Sec. II. These two correlation functions are directly related to the distance correlation function characterizing the intrachain motion, and thus provide experimentally reliable measures to probe the conformational dynamics. Furthermore, each measurement of the donor–acceptor distance in real experiments corresponds to a large number of polymer configurations. To differentiate them, the instantaneous diffusion coefficient is calculated in Sec. IV C to probe the variation of the donor–acceptor distance with time, and yielding information about the mean square distance as well as instantaneous distance between the dye molecules.

To model FRET experiments, we treat the reaction dynamics as a convolution of the polymer motions and the actual energy transfer event which depends on the separation between probes. Without the intrachain motion, each fluorescence lifetime τ corresponds to a specific donor–acceptor distance R_{nm}. And the fluorescence lifetime distribution function directly reflects the equilibrium distribution of intrafluorophore distance.[12] However, the slow intrachain dynamics slightly modifies this correspondence and brings another configuration-dependent weighting factor. In Sec. V, the FRET lifetime in the fast reaction limit is discussed to incorporate the intrachain motion during the energy transfer reaction. Inhomogeneous cumulant expansion of τ leads to a weighted inhomogeneous reaction time, which serves as a perturbative correction to the static lifetime $\tau=K^{-1}$. Thus through single-molecule lifetime measurements one can map out the distance distribution function even with intrachain relaxation.

The single-molecule spectroscopy and imaging directly track the Brownian dynamics of polymers in solution, which determines the viscoelasticity property from the correlation function of single molecules. The single-molecule approach has become known as microrheology in analogy to rheology, which studies the viscoelasticity behavior through the response of the bulk material to applied mechanical perturbation.[30,31] Evidently, rheology and microrheology measurements are related to each other, and this relationship will be explained in Sec. VI through the example of the intrinsic viscosity. The theoretical calculation of polymer viscosity has a long history, ranging from Kirkwood's classical treatment, to the formulation by Fixman, Bixon and Zwanzig, etc.[32,35–37] In Sec. VI, we relate the correlation function of intrachain dynamics on the single polymer to intrinsic viscosity and evaluate the viscosity explicitly with the consideration of the persistence length. Our expression for the intrinsic viscosity is related to the correlation function formula discussed by Felderhof, Deutch, and Titulaer,[38] but is further simplified for the application to single-molecule measurements of Gaussian chain dynamics.

II. SEMIFLEXIBLE GAUSSIAN CHAINS

Before calculating the dynamics, we first develop the Gaussian model with a persistence length. Consider a discretized version of a continuous polymer chain without explicit account of the excluded volume effects. The nth unit of the polymer is at a position denoted $\mathbf{r}_n$. The bond vector $\mathbf{u}_n=\mathbf{r}_n-\mathbf{r}_{n-1}$ separates two neighboring units of the polymer chain. It should be noted that the bond vector does not correspond to an actual chemical bond nor do the subunits correspond to a single monomer.

Although the focus of this paper will be on single polymer dynamics, we start by examining the equilibrium distribution of the polymer chain. Averaging $\mathbf{u}$ and $\mathbf{u}^2$ over all possible orientations gives $\langle\mathbf{u}_n\rangle=0$ and $\langle\mathbf{u}_n^2\rangle=a_0^2$ with a_0 the bond length. To describe the rigidity of the polymer chain, we define the correlation between two bonds as $\langle\mathbf{u}_n\mathbf{u}_m\rangle=a_0^2b^{|n-m|}$ with $0<b<1$. If $b=1$, every $\mathbf{u}_n$ must point in the same direction resulting in a rigid rod. If $b=0$, there is no correlation between two bond vectors and the chain is an ideal Gaussian chain on all length scales. The total length of the polymer is the sum of all the individual bond vectors, $\mathbf{R}=\Sigma_{n=1}^{N-1}\mathbf{u}_n$, where $N-1$ is the number of bond vectors. Using the relations between bond vectors we have $\langle\mathbf{R}\rangle=0$ and

$$\langle\mathbf{R}^2\rangle=\sum_{nm}\langle\mathbf{u}_n\mathbf{u}_m\rangle=\left[\frac{(1+b)}{(1-b)}(N-1)-2b\,\frac{(1-b^{N-1})}{(1-b)^2}\right]a_0^2. \tag{1}$$

In most applications to polymers the second term would be neglected because of the large N limit, which gives us the expected result $\langle\mathbf{R}^2\rangle=L_k(N-1)a_0^2$, where $L_k=(1+b)/(1-b)$ is the Kuhn length. The persistence length is related to the Kuhn length by $L_p=L_k/2$. Taking the continuous limit of the discretized model we have $b=\exp(-1/L_p)$ and $\langle\mathbf{u}(s)\mathbf{u}(s')\rangle=a_0^2\exp(-|s-s'|/L_p)$, where the variables s and s' are the continuous analog of the index for the subunits and allow us to trace the positions of the subunits on the polymer. In the continuous limit, the expression for $\langle\mathbf{R}^2\rangle$ becomes

$$\langle \mathbf{R}^2 \rangle = \int_0^{N-1} \int_0^{N-1} ds\, ds' \exp(-|s-s'|/L_p)$$
$$= 2a_0^2 L_p (N-1) - 2a_0^2 L_p^2 [1 - e^{-(N-1)/L_p}]. \quad (2)$$

For the long chain length limit we get the expected scaling relation for a random Gaussian chain $\langle \mathbf{R}^2 \rangle = 2(N-1)L_p a_0^2$. In the short chain length limit, we also have the expected relationship for a rigid rod $\langle \mathbf{R}^2 \rangle = (N-1)^2 a_0^2$.

It is known that the Gaussian process with exponential-decay correlation defines the Ornstein–Uhlenbeck process. The three-dimensional equilibrium distribution function is denoted as $P_{\mathrm{eq}}(\mathbf{u}) \propto \exp[-\beta U]$ with the exponential functional given by

$$\beta U(\mathbf{u}) = \frac{3}{2a_0^2(1-b^2)} \sum_{n=1}^{N-2} (\mathbf{u}_{n+1} - b\mathbf{u}_n)^2 + \frac{3\mathbf{u}_1^2}{2a_0^2}, \quad (3)$$

where U is understood as the potential energy of the Gaussian chain. For the purpose of further calculations, the potential function can be cast into

$$\beta U = \frac{3}{2a_0^2(1-b^2)} \sum_{n=1}^{N-2} \left[\left(\frac{1+b}{2} \right)^2 (\mathbf{u}_{n+1} - \mathbf{u}_n)^2 + (1-b)^2 \left(\frac{\mathbf{u}_{n+1} + \mathbf{u}_n}{2} \right)^2 \right] + \frac{3}{4a_0^2} (\mathbf{u}_{N-1}^2 + \mathbf{u}_1^2)$$
$$= \frac{3}{4a_0^2} \sum_{n=1}^{N-2} \left[L_p (\mathbf{u}_{n+1} - \mathbf{u}_n)^2 + \frac{1}{L_p} \left(\frac{\mathbf{u}_{N+1} + \mathbf{u}_n}{2} \right)^2 \right] + \frac{3}{4a_0^2} (\mathbf{u}_{N-1}^2 + \mathbf{u}_1^2), \quad (4)$$

where L_p is the persistence length defined earlier. Note the extra terms for the initial and final vectors $\mathbf{u}_1$ and $\mathbf{u}_{N-1}$ in Eq. (4) are necessary for satisfying the chain homogeneity, i.e., the length of each bond is constant on average. The Boltzmann distribution generated from this potential function rigorously reproduces the Gaussian statistics as introduced in Eq. (1). For a long Gaussian chain, we take the continuous limit as

$$\beta U[\mathbf{u}(s)] = \frac{3}{4a_0^2} \left[\int_0^{N-1} ds\, L_p \left(\frac{\partial \mathbf{u}}{\partial s} \right)^2 + \frac{1}{L_p} \mathbf{u}^2 \right] + \frac{3}{4a_0^2} (\mathbf{u}_{N-1}^2 + \mathbf{u}_1^2), \quad (5)$$

where the bond index is treated as a continuous variable. Clearly, from Eq. (5), the semiflexible model exhibits the same long chain asymptotic behavior as the original Rouse modes as well as the proper behavior for a stiff rod on shorter length scales.

Similar results have also been obtained by Winkler, Reineker, and Harnau[39] using the maximum entropy method and by Ha and Thirumalai[27] using a mean-field approach. As noted by Lagowski, Noolandi, and Nickel,[40] the Gaussian chain thus generated is homogeneous and has an exponential decay correlation, which are the properties of the Ornstein–Uhlenbeck process. Earlier adaptations of the process to stiff chains treat the boundaries differently and do not lead to the chain homogeneity implied in the Gaussian statistics.

III. BROWNIAN DYNAMICS OF SEMIFLEXIBLE CHAINS

Single-molecule experiments measure trajectories of intrachain motions of polymers, and the interpretation of such measurements is helped by model calculations of polymer dynamics. The Brownian motion of a polymer chain is governed by the Langevin equation for each bead,

$$\zeta \dot{\mathbf{r}}_n = -\nabla_n U + \mathbf{f}_n, \quad (6)$$

where $\mathbf{f}_n$ is the random force with local Gaussian distribution, $\langle \mathbf{f}_n(t) \rangle = 0$, $\langle f_{n\alpha}(t) f_{m\beta}(t') \rangle = 2\zeta k_B T \delta_{mn} \delta_{\alpha\beta} \delta(t-t')$. Although the equations of motion are straightforward, the solutions to these equations are not trivial. To make the problem more tractable, we define normal modes so that the dynamics of each mode are independent and the equations of motion for these modes are simplified. For the flexible Gaussian polymer chain, one usually defines the Rouse normal modes, which have a Fourier decomposition into functions of the form $\cos(\pi pn/N)$, where n is the bead index, N is the total number of beads, and p is an integer denoting the normal modes. The $\sin(\pi pn/N)$ components are zero by the requirement that the derivative be zero at the end points of the polymer chain. Because the applications that we are examining are for semiflexible chains, it is advantageous to modify the Rouse mode to treat the end units more rigorously. The normal modes are defined as

$$\mathbf{r}_n = \mathbf{x}_0 + 2 \sum_{p=1}^{N-1} \mathbf{x}_p \cos\left[\left(n - \frac{1}{2} \right) \frac{p\pi}{N} \right], \quad (7)$$

where p is an integer denoting the modes. This definition removes the artificial constraint on the end point derivatives previously imposed in the Rouse normal mode decomposition. For the semiflexible Gaussian chain, the normal modes defined in Eq. (7) approximately diagonalize the potential and simplify the dynamics of the polymer chain (see Appendix A). The equation of motion for the pth mode becomes

$$\zeta_p \frac{\partial \mathbf{x}_p}{\partial t} = -\lambda_p \mathbf{x}_p + \mathbf{f}_p, \quad (8)$$

where

$$\lambda_p = \frac{24 N k_B T}{a_0^2} \sin^2 \frac{p\pi}{2N} \left(2L_p \sin^2 \frac{p\pi}{2N} + \frac{1}{2L_p} \cos^2 \frac{p\pi}{2N} \right), \quad (9)$$

$$\zeta_p = 2N\zeta - \delta_{0,p} N\zeta, \quad (10)$$

$$\langle f_{p\alpha}(t) f_{q\beta}(t') \rangle = 2\delta_{pq} \delta_{\alpha\beta} \zeta_p k_B T \delta(t-t'). \quad (11)$$

Evidently, the random force acts on each mode independently and satisfies the fluctuation–dissipation relation.

The concept of normal modes in polymer dynamics has been directly applied to the interpretation of single-molecule experiments. For example, Winkler has calculated the normal mode relaxation dynamics of stretched flexible chain molecules,[41] which agrees with Chu's experimental data.[17] In the limit $L_p \to 1/2$, the above-given normal modes recover the Rouse model discussed in standard textbooks.[29] For a

rigid-rod like polymer, $L_p \to \infty$, all the normal modes will be suppressed, keeping only the center of mass motion. Exact numerical solution of the original equation of motion in Eq. (6) will keep both the transnational and rotational motion of the rigid rod.

Through the Brownian dynamics of the semiflexible chain, one can relate single-molecule FRET measurements to the correlations between the sites on the polymer chain where two dye molecules are attached. We define the distance between the two beads on the polymer chain $\mathbf{R}_{nm} = \mathbf{r}_n - \mathbf{r}_m$, where m and n correspond to the index of the two points on the polymer chain. In terms of normal modes we can express this quantity as

$$\mathbf{R}_{nm} = \sum_{p=1}^{N-1} c_{nm}^p \mathbf{x}_p$$

with

$$c_{nm}^p = -4 \sin \frac{p\pi}{2N}(n-m) \sin \frac{p\pi}{2N}(n+m-1). \tag{12}$$

The propagation of the normal modes follows the Smoluchowski equation in a quadratic potential (see Appendix A). The correlation between $\mathbf{R}_{nm}(0)$ and $\mathbf{R}_{nm}(t)$ is

$$\langle \mathbf{R}_{nm}(t) \cdot \mathbf{R}_{nm}(0) \rangle = \sum_{p=1}^{N-1} (c_{nm}^p)^2 \frac{3k_BT}{\lambda_p} \exp\left[-\frac{\lambda_p}{\zeta_p} t \right]. \tag{13}$$

At $t=0$, the above-noted expression gives the mean square distance between the nth and the mth beads along the chain, R_{nm}^2, as is given in Eq. (B4). Direct evaluation of the sum in the equation is plotted in Fig. 1, where R_{nm}^2 shows a quadratic dependence on $|n-m|$ for small $|n-m|$ and a linear dependence on $|n-m|$ for large $|n-m|$.

(1) In the short time region, summation over the first-order Taylor expansion of each exponential function leads to

$$\langle \mathbf{R}_{nm}(t) \cdot \mathbf{R}_{nm}(0) \rangle = \langle \mathbf{R}_{nm}^2 \rangle - 6Dt,$$

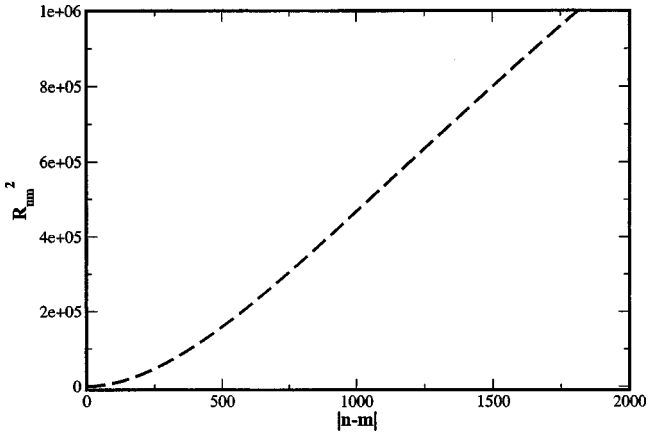

FIG. 1. The mean square distance between the nth and the mth beads given in Eq. (14) for a polymer chain with 5000 beads. Here a_0 is taken as the unit length and the persistence length L_p is taken as 500. As shown in Eq. (C6), R_{nm}^2 has a quadratic dependence on $|n-m|$ for $|n-m| \ll L_p$, and is proportional to $|n-m|$ for $|n-m| \gg L_p$.

with

$$D = \frac{k_BT}{\zeta}, \tag{14}$$

so each bead undergoes instantaneous diffusive motion in three-dimensional space without feeling the interaction of the polymer chain. This short time behavior does not depend on the persistence length and exists in the ideal Rouse chain as well.

(2) In the intermediate time region, each normal mode decays with various rates, and contributes jointly to the correlation function $\langle \mathbf{R}_{nm}(t) \cdot \mathbf{R}_{nm}(0) \rangle$. For different degrees of stiffness, the correlation function has different time scales. In the large N limit, the summation over p can be approximated by an integral from 1 to infinity, resulting in

$$\langle \mathbf{R}_{nm}(t) \cdot \mathbf{R}_{nm}(0) \rangle = \begin{cases} \dfrac{2a_0^2}{\pi} L_p^{3/2} (n-m)^2 t^{*-1/2} \Gamma\left(\dfrac{1}{2}, \dfrac{\pi^2 t^*}{4N^2 L_p} \right), & L_p \ll N \\ \dfrac{a_0^2}{2\sqrt{2}\pi} L_p^{-3/4} (n-m)^2 t^{*1/4} \Gamma\left(-\dfrac{1}{4}, \dfrac{\pi^4 L_p t^*}{4N^4} \right), & L_p \gg N, \end{cases} \tag{15}$$

where $t^* = 6Dt/(a_0^2)$ is the reduced time, and $\Gamma(\alpha, z) = \int_z^\infty x^{\alpha-1} \exp(-x) dx$ is the incomplete gamma function. As shown in Fig. 2, the normalized distance correlation function $\phi(t) = \langle \mathbf{R}_{nm}(t) \cdot \mathbf{R}_{nm}(0) \rangle / \langle \mathbf{R}_{nm}^2 \rangle$ decays nonexponentially for both flexible and stiff chains. The decay time increases with the persistence length.

(3) In the long time region, only the slowest mode survives, and the correlation function becomes

$$\langle \mathbf{R}_{nm}(t) \cdot \mathbf{R}_{nm}(0) \rangle = (c_{mn}^1)^2 \frac{3k_BT}{\lambda_1} \exp\left[-\frac{\zeta_1}{\lambda_1} t \right], \tag{16}$$

which represents the fundamental relaxation mode of the polymer chain.

At this point, the model that we have constructed is similar to the Rouse model, where the only interactions are those dictated by the connectivity of the polymer. It is known that the Rouse model does not reproduce experimental results because spatial interactions between two monomers separated by large distances along the polymer backbone are important. To develop a more realistic polymer model, we should include real polymer interactions like hydrodynamic and excluded volume effects. These effects can be included

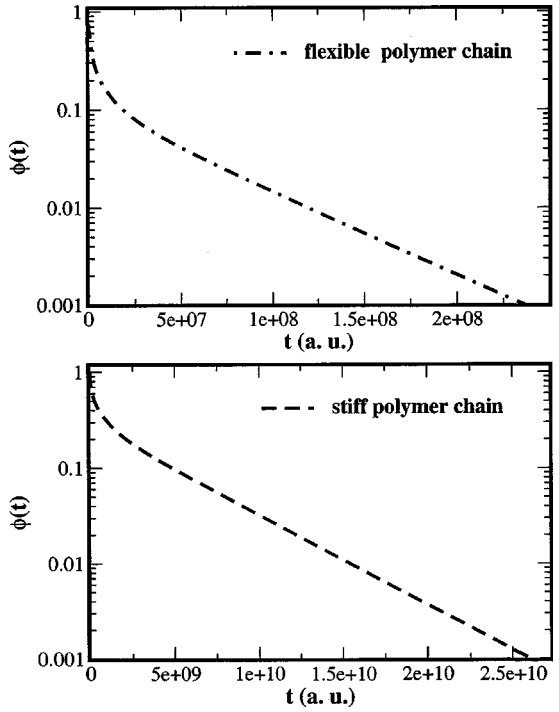

FIG. 2. Log plot of the normalized distance correlation function $\phi(t)$ for a polymer chain with 5000 beads. $L_p=5$ for the flexible chain and $L_p=500$ for the stiff chain. $\zeta a_0^2/6k_BT$ is taken as the time unit. $\phi(t)$ decays nonexponentially with time. Obviously $\phi(t)$ decays on a much longer time scale for the stiff chain than for the flexible chain.

by similar approximations introduced in the Zimm model. We discuss hydrodynamic interactions briefly in Appendix D.

From the above-mentioned analysis, it is apparent to note that the interfluorophore distance $\mathbf{R}_{nm}$ follows an effective diffusion process, with the Green's function in Eq. (B8) characterizing a Gaussian process with nonexponential correlation. $\int_0^\infty \phi(t)dt$ provides a time scale for the effective diffusion, the effective diffusion coefficient in the potential of mean force can be formulated as $6D_{\text{eff}}\int_0^\infty \phi(t)dt=\langle \mathbf{R}_{nm}^2\rangle$, which is generally different from the diffusion coefficient $2D$ used in Pastor, Zwanzig, and Szabo's work,[42] where $D=k_BT/\zeta$ is the diffusion coefficient for each polymer bead. As discussed later in Sec. IV C, the diffusion coefficient $2D$ only reflects the diffusive motion of each polymer bead independently and contains no information about the collective motion of the polymer chain.

IV. SINGLE-MOLECULE FRET OF SEMIFLEXIBLE CHAINS

Single-molecule fluorescence resonant energy transfer (FRET) allows us to measure the separation of donor and acceptor dye pairs on a single polymer chain. In a simple experimental setup, the donor and acceptor are located on specific sites on the polymer chain. According to Förster theory, resonant energy transfer is mediated by the dipole–dipole interaction, and the transfer rate depends on the donor–acceptor separation as $K(R)\propto 1/R^6$. The inverse sixth-power law leads to a sensitive probe of intrachain dynamics, which has been exploited extensively in recent single-molecule experiments. To interpret the FRET experiments and extract the desired information, we calculate single-molecule quantities for the intrapolymer energy transfer process, which is controlled by the polymer conformations.

A. Distribution and correlation function of FRET efficiency

With the help of two photon-counting detection channels, one can track the real-time evolution of intramolecular and intermolecular distances of a freely diffusing individual macromolecule.[8] The instantaneous FRET efficiency $E(t)$ is calculated from the donor and acceptor emission intensities I_d and I_a, using the formula $E=[1+\gamma I_d/I_a]^{-1}$, where γ is a correction factor. According to the Förster theory, the efficiency E has a strong dependence on the interfluorophore distance, $E=[1+(R/R_F)^6]^{-1}$, where R_F is the Förster radius. The Förster energy transfer occurs on the nanosecond scale, whereas conformational changes of polymers usually occur on the millisecond scale or even longer. Therefore the donor and acceptor fluorophores quickly reach kinetic equilibrium under a laser pump, and hence the efficiency E provides ''snapshots'' of the polymer configurations over time. The correlation of the FRET efficiency, defined as,

$$C_{nm}(t)=\frac{\langle E(t)E(0)\rangle-\langle E\rangle^2}{\langle E^2\rangle-\langle E\rangle^2}, \tag{17}$$

provides additional information on conformational dynamics on a large time scale that is difficult, and sometimes impossible, to obtain by conventional techniques.[9]

For the semiflexible Gaussian chain introduced in Sec. II, we evaluate the correlation function explicitly. Assuming that the donor and acceptor dye molecules are attached to the nth and the mth beads of a single semiflexible polymer chain, the FRET efficiency E is related to the interfluorophore distance R_{nm} by

$$E(R_{nm})=\frac{1}{1+(R_{nm}/R_F)^6}. \tag{18}$$

The interfluorophore distance R_{nm} is governed by the Brownian motion of the polymer chain. The equilibrium distribution and evolution derived in Appendix B are

$$P_{\text{eq}}(\mathbf{R}_{nm})=\left[\frac{2\pi}{3}\langle \mathbf{R}_{nm}^2\rangle\right]^{-3/2}\exp\left\{-\frac{3\mathbf{R}_{nm}^2}{2\langle \mathbf{R}_{nm}^2\rangle}\right\}, \tag{19}$$

$$G(\mathbf{R}_{nm}(t),t|\mathbf{R}_{nm}(0))=\left[\frac{2\pi}{3}\langle \mathbf{R}_{nm}^2\rangle(1-\phi(t)^2)\right]^{-3/2}\times\exp\left\{-\frac{3(\mathbf{R}_{nm}(t)-\phi(t)\mathbf{R}_{nm}(0))^2}{2\langle \mathbf{R}_{nm}^2\rangle(1-\phi(t)^2)}\right\}, \tag{20}$$

where $\phi(t)$ is the normalized correlation function of the interfluorophore distance given in Eq. (B5). Thus the average efficiency and the correlation function can be explicitly evaluated as

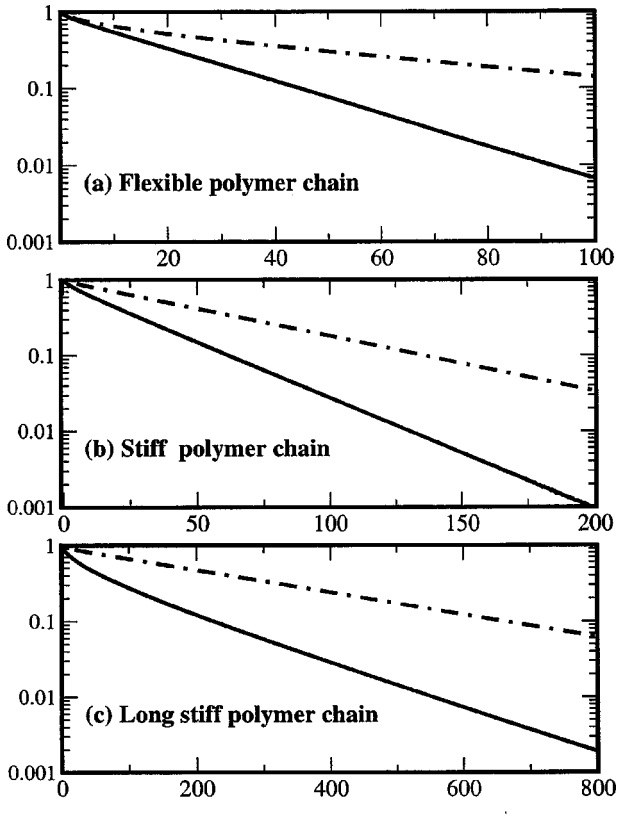

FIG. 3. Comparison of the FRET efficiency correlation function $C_{nm}(t)$ for various $\langle R_{nm}^2\rangle$. a_0 and $\zeta a_0^2/6k_BT$ are taken as the length unit and the time unit, respectively. The Förster radius R_F is taken to be 5. The solid lines are the efficiency correlation functions, and the dot-dashed lines are the corresponding distance–distance correlation function $\phi(t)$. (a) Flexible chains with $N=10$, $L_p=0.5$. (b) Stiff chains with $N=10$, $L_p=2.0$. (c) Long stiff chains with $N=20$, $L_p=2.0$.

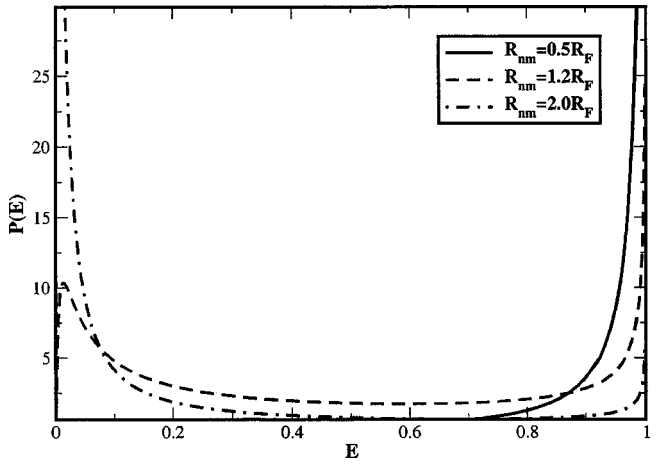

FIG. 4. The distribution of the FRET efficiency with the Förster radius R_F as the length unit. $R_{nm}=|\mathbf{R}_{nm}|$ is the mean square root of the donor–acceptor distance. As R_{nm} increases from $0.5R_F$ to $2.0R_F$, the distribution shifts from the unimodal distribution around $E=1$, to the bimodal distribution, and then to the unimodal distribution around $E=0$.

$$\langle E\rangle=\int d^3\mathbf{R}_{nm}E(R_{nm})P_{\mathrm{eq}}(\mathbf{R}_{nm}),$$

$$C_{nm}(t)=\int\int d^3\mathbf{R}_{nm}(t)d^3\mathbf{R}_{nm}(0)E(R_{nm}(t))E(R_{nm}(0))\times G(\mathbf{R}_{nm}(t),t|\mathbf{R}_{nm}(0))P_{\mathrm{eq}}(\mathbf{R}_{nm}). \quad (21)$$

For small R_F, we can approximate Eq. (18) as a delta function and show that

$$\langle E\rangle\propto\left[\frac{\langle R_{nm}^2\rangle}{R_F^2}\right]^{-3/2}, \quad (22)$$

$$C_{nm}(t)\sim[1-\phi^2(t)]^{-3/2}-1. \quad (23)$$

In real experiments, the FRET efficiency measurement is mainly performed in the regime where $R_{nm}\leqslant R_F$ and the efficiency is sensitive to the interfluorophore distance only in the close vicinity of R_F. Although it is difficult to obtain the analytical expression of the FRET efficiency correlation function under such condition, a numerical example plotted in Fig. 3 still shows the close relation between $C_{nm}(t)$ and $\phi(t)$. We have plotted three different cases in Fig. 3, $\langle R_{nm}^2\rangle\ll R_F^2$ for a flexible chain, $\langle R_{nm}^2\rangle\sim R_F^2$ for a short stiff chain, and $\langle R_{nm}^2\rangle\gg R_F^2$ for a long stiff chain. In the short time limit, $C_{nm}(t)$ is a combination of all the relaxation modes, while in the long time limit, only the fundamental mode exists. As shown in Fig. 3, $C_{nm}(t)$ always decays on the same time scale as that of $\phi(t)$ for various stiffness and chain lengths, thus providing a good probe of the intrachain dynamics.

Besides the FRET efficiency correlation function, the distribution function of the efficiency is also a good measure of the chain stiffness. In general, the efficiency distribution is obtained by transforming the equilibrium distribution of R_{nm} into the efficiency E of Eq. (18) as

$$P(E)=\sqrt{\frac{3}{2\pi}}\frac{R_F^3}{\langle\mathbf{R}_{nm}^2\rangle^{3/2}}(1-E)^{-1/2}E^{-3/2}\times\exp\left[-\frac{3R_F^2}{2\langle\mathbf{R}_{nm}^2\rangle}\left(\frac{1-E}{E}\right)^{1/3}\right]. \quad (24)$$

As shown in Fig. 4, plots of the efficiency distribution with different mean square interfluorophore distance display different features. As the mean square interfluorophore distance increases, the FRET efficiency sharply shifts from the unimodal peak at $E=1$, to the bimodal distribution, and then to the unimodal peak at $E=0$. These features are explored numerically by Srinivas and Bagchi to distinguish the disordered and ordered conformations.[43] The complicated feature of the efficiency distribution implies that the average efficiency $\langle E\rangle$ does not provide enough information of the distribution.

In a recent experiment, Weiss and co-workers investigated the single enzyme Staphylococcal nuclease with FRET. The instantaneous FRET efficiencies $E(t)$ and the correlation functions $C_{nm}(t)$ were evaluated for 100 labeled Staphylococcal nuclease molecules.[9] It was observed that the correlation functions had a wide distribution of time constants, which demonstrates the complexity of the intrachain motion.

B. Correlation of FRET lifetime

Optical methods developed recently are capable of tracking single molecules under physiological conditions in real time. The environmental changes of individual molecules induce the conformational changes of molecular configurations on a much longer time scale than energy transfer. As a result, the dynamical tracking of lifetime information provides a measure of individual molecules in nonequilibrated and heterogeneous systems, and offers details of single-molecule dynamics that are usually hidden in conventional ensemble measurements.

The decay of the fluorescence on the donor includes radiative decay and nonradiative energy transfer,

$$K=\frac{1}{\tau_D}\left[1+\left(\frac{R_{nm}}{R_F}\right)^{-6}\right], \tag{25}$$

where R_F is the Förster radius and τ_D is the fluorescence lifetime without acceptor. Since the intrachain dynamics occurs on a much longer time scale than the FRET process, the polymer configuration remains the same when the FRET occurs, hence the lifetime is a ''snapshot'' at the transient conformation,

$$\tau \approx \frac{1}{K}=\frac{\tau_D}{1+(R_{nm}/R_F)^{-6}}. \tag{26}$$

Continuous ''snapshots'' of transient configurations reveal the correlation between two configuration-controlled lifetimes, which reflects the slow intrachain motion that modifies the donor–acceptor distance R_{nm}. The lifetime correlation function is defined as

$$C_{nm}(t)=\frac{\langle \tau(t)\tau(0)\rangle-\langle\tau\rangle^2}{\langle\tau^2\rangle-\langle\tau\rangle^2}, \tag{27}$$

where $\langle\cdots\rangle$ is the average over various initial configurations of a given pair, and the configuration-controlled lifetime τ is related to the energy transfer efficiency E discussed in Sec. IV A as $\tau=\tau_D(1-E)$. Therefore, the lifetime correlation function is exactly the same as the efficiency correlation function in Eq. (17), which can be used to monitor the intrachain dynamics at the single-molecule level.

The efficiency measurement discussed in Sec. IV A and the lifetime measurement determine similar quantities. Both measurements utilize the separation of the time scales for the reaction and the diffusion processes to detect the dynamical evolution of microenvironments at the single-molecule level. The lifetime method requires only one detection channel but with high time resolution usually in nanosecond scale, while the efficiency measurement requires simultaneously tracking donor and acceptor emissions but with relatively lower time resolution. Both methods are experimentally reliable for monitoring the intrachain motion in real time.

C. Instantaneous diffusion coefficient

In FRET measurements, the experimental sample with the attached donor and acceptor dyes is either adsorbed to the glass surface or prepared in solution. Fluorescence images of the sample are detected by scanning the confocal volume, and photobleaching curves of donor and acceptor are simultaneously recorded with an integration time t_{bin}. As a result, the trajectories of the distance between two dyes are obtained. Each measurement of the interfluorophore distance R_{nm} can correspond to a large number of polymer configurations. To differentiate them, the variation of the distance with respect to time is examined in order to understand the dynamic heterogeneity of structure.[11] The instantaneous diffusion coefficient measured in these experiments is defined as

$$\bar{D}(R_{nm}(0))=\frac{1}{6t_{\mathrm{bin}}}\langle(\mathbf{R}_{nm}(t_{\mathrm{bin}})-\mathbf{R}_{nm}(0))^2\rangle_G, \tag{28}$$

where t_{bin} is the experimental bin time due to the finite time resolution and $\langle\cdots\rangle_G$ stands for the integration over the Green's function for a fixed initial separation $R_{nm}(0)$. For the semiflexible polymer chain, we are able to evaluate instantaneous diffusion coefficient directly with the Green's function in Appendix B, giving

$$\bar{D}(R_{nm}(0))=\langle\mathbf{R}_{nm}^2\rangle\frac{1-\phi^2(t_{\mathrm{bin}})}{6t_{\mathrm{bin}}}+\mathbf{R}_{nm}^2(0)\frac{[1-\phi(t_{\mathrm{bin}})]^2}{6t_{\mathrm{bin}}}. \tag{29}$$

This expression of $\bar{D}(R_{nm}(0))$ is a general result for any Gaussian process and implies the following:

(1) As t_{bin} approaches 0, only the first term survives and the instantaneous diffusion coefficient reduces to $2D=2k_BT/\xi$, which describes the independent diffusive motions of the donor and acceptor sites and does not provide any information of the chain-configurations or the interactions.

(2) As t_{bin} approaches ∞, averaging Eq. (29) over the initial position $\mathbf{R}_{nm}(0)$ yields the relation in the long time limit, $6\bar{D}t_{\mathrm{bin}}=2\langle\mathbf{R}_{nm}^2\rangle=\langle(\mathbf{R}_{nm}(t_{\mathrm{bin}})-\mathbf{R}_{nm}(0))^2\rangle$, where $\bar{D}$ is the diffusion coefficient of polymer beads.

(3) The mean square distance in equilibrium $\langle\mathbf{R}_{nm}^2\rangle$, which is determined by the morphological structures of the polymer, relies on the condition of the solution. $\langle\mathbf{R}_{nm}^2\rangle$ in the collapsed state is smaller than that in the coiled state, and $\langle\mathbf{R}_{nm}^2\rangle$ in the coiled state is much smaller than that in the ordered state (rod, toroidal, etc.). As a result, $\bar{D}(R_{nm}(0))$ in collapsed structures is much smaller than that in coiled structures.

(4) For a specific condition of solution when the mean square distance in equilibrium $\langle\mathbf{R}_{nm}^2\rangle$ is fixed, the variation of $\bar{D}(R_{nm}(0))$ has a quadratic dependence on the initial distance $R_{nm}(0)=|\mathbf{R}_{nm}(0)|$.

These conclusions are in qualitative agreement with recent experiments on PCN-4.[11] Instead of two fluorophores attached to the same chain, the donor and acceptor dye molecules in the reported experiment are attached to each end of a double helix DNA molecule, respectively. Therefore the quadratic dependence on $R_{nm}(0)$ is not exactly observed. It was observed that the instantaneous diffusion coefficient in the unfolded state is one order of magnitude greater than that in the folded condition, which means $\langle\mathbf{R}_{nm}^2\rangle$ in the folded state is much smaller than that in the unfolded state.

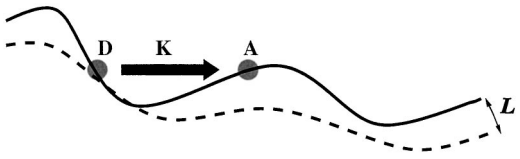

FIG. 5. A sketch of intrachain fluorescence resonant energy transfer process, with double arrow denoting the intrachain dynamics $\mathcal{L}$, and with thick arrow denoting the population depletion from the donor.

V. THE FRET LIFETIME DISTRIBUTION

In order to calculate the lifetime distribution, we consider a general scenario where the kinetics of the system described by

$$\dot{P}(t)=\mathcal{L}P(t)-KP(t), \tag{30}$$

where $P([\mathbf{r}],t)$ is the probability distribution function of the polymer chain and $\mathcal{L}$ is the propagation operator of the chain. As illustrated in Fig. 5, the depletion of the population is denoted by K and the intrachain motion is governed by $\mathcal{L}$. At zero time, we pump the donor dye to an excited state, and then monitor the lifetime distribution. The Laplace transform of Eq. (30) yields

$$\hat{P}(z)=\frac{1}{z-\mathcal{L}+K}P_0, \tag{31}$$

where $\hat{P}(z)$ is the Laplace transform of $P(t)$ and P_0 is the initial population. To calculate the lifetime distribution function, we take the average of Eq. (31) over the equilibrium distribution P_{eq} and obtain the equation for the survival probability $\hat{N}(z)=\langle(z-\mathcal{L}+K)^{-1}\rangle$, where the angular brackets $\langle\cdots\rangle$ refer to the configurational average over the equilibrium distribution function P_{eq}, i.e., $\langle A\rangle=\int AP_{\mathrm{eq}}d^N\mathbf{r}$. From $\hat{N}(z)$ we calculate the Laplace transform of the ensemble lifetime distribution as

$$\hat{f}(z)=1-z\hat{N}(z)=\langle(K-\mathcal{L})(z-\mathcal{L}+K)^{-1}\rangle. \tag{32}$$

In the sluggish environment, $\mathcal{L}\ll K$, the relaxation of the reactive system is extremely slow so that the reaction rate depends only on the transient configuration, therefore, the lifetime is $\tau=\hat{P}(0)\approx K^{-1}$. The survival probability in Laplace space becomes $N(z)\approx\langle(z+K)^{-1}\rangle$, and the lifetime distribution function is the static average over the equilibrium configuration, i.e.,

$$f(t)=\int Ke^{-Kt}P_{\mathrm{eq}}d^N\mathbf{r}. \tag{33}$$

Under such conditions, the interfluorophore distance distribution as well as the transfer rate distribution can be obtained from single-molecule fluorescence lifetime measurements.[12] The ensemble averaged lifetime becomes the static average of the inhomogeneous lifetime τ, $\langle t\rangle\approx\langle K^{-1}\rangle$.[44]

However, natural functions of biological polymers are usually studied in solutions, where the static limit in Eq. (33) does not apply. Although the energy transfer reaction occurs on a faster time scale than the intrachain relaxation, it is important to include the relaxation effects in the lifetime distribution function. To take into account the polymer motion during the reaction, $\hat{P}(z)$ can be evaluated with inhomogeneous cumulant expansion for a fixed initial configuration which has been used in studying spectral diffusion,[45] giving

$$P(\mathbf{R}_0,t)=\left\langle \exp\left(-\int_0^t K(\tau)d\tau\right)\right\rangle_{\mathbf{R}_0}. \tag{34}$$

Here $\langle\cdots\rangle_{\mathbf{R}_0}$ stands for the homogeneous average for a fixed initial configuration and can be calculated with cumulant expansion, for example, to first order, as

$$P(\mathbf{R}_0,t)\approx\exp\left[-\int_0^t\langle K(\tau)\rangle_{\mathbf{R}_0}d\tau\right]. \tag{35}$$

For the semiflexible chain model introduced in Sec. II, the inhomogeneous average is performed over the Green's function in Eq. (B7), giving

$$\begin{aligned}\langle K(\tau)\rangle_{\mathbf{R}_0}&=\int\frac{K(\tilde{\mathbf{R}}+\mathbf{R}_0\phi(t))}{[2\pi\langle\mathbf{R}_{nm}^2\rangle(1-\phi(t)^2)/3]^{3/2}}\\&\quad\times\exp\left[-\frac{3\tilde{\mathbf{R}}^2}{2\langle\mathbf{R}_{nm}^2\rangle(1-\phi(t)^2)}\right]d^3\tilde{R}\\&\approx K(\mathbf{R}_0)+2Dt\sum_\mu\partial_\mu\partial_\mu K(\mathbf{R}_0),\end{aligned} \tag{36}$$

where we have applied the short time expansion of $K(\tilde{\mathbf{R}}+\mathbf{R}_0\phi(t))\approx K(\mathbf{R}_0)+\Sigma_{\mu,\nu}\partial_\mu\partial_\nu K(\mathbf{R}_0)\tilde{R}_\mu\tilde{R}_\nu/2$ with μ, ν standing for x, y, z, $\langle\mathbf{R}_{nm}^2\rangle(1-\phi(t)^2)\approx 12Dt$, and $D=k_BT/\zeta$. Therefore Eq. (35) can be approximated as

$$\begin{aligned}P(\mathbf{R}_0,t)&\approx\exp\left[-K(\mathbf{R}_0)t-D\sum_\mu\partial_\mu\partial_\mu K(\mathbf{R}_0)t^2\right]\\&\approx\exp\left[-K(\mathbf{R}_0)t-\frac{D\Sigma_\mu\partial_\mu\partial_\mu\partial_\mu K(\mathbf{R}_0)}{K(\mathbf{R}_0)^2}\right],\end{aligned} \tag{37}$$

where in the second approximation t is replaced by the reaction time $1/K(\mathbf{R}_0)$ for a specific configuration in the fast reaction limit. Thus the lifetime

$$\tau\approx\frac{1}{K(\mathbf{R}_0)}\exp\left[-\frac{D\Sigma_\mu\partial_\mu\partial_\mu\partial_\mu K(\mathbf{R}_0)}{K(\mathbf{R}_0)^2}\right] \tag{38}$$

becomes a weighted inhomogeneous reaction time and the lifetime distribution becomes a weighted average over inhomogeneous configurations,

$$f(t)=\int K(\mathbf{R}_0)\exp\left[-\frac{D\Sigma_\mu\partial_\mu\partial_\mu\partial_\mu K(\mathbf{R}_0)}{K(\mathbf{R}_0)^2}\right]P_{\mathrm{eq}}(\mathbf{R}_0)d^3R_0. \tag{39}$$

For the FRET rate described in Eq. (25), the weighting factor can be evaluated explicitly as

$$\begin{aligned}&\exp\left[-\frac{D\Sigma_\mu\partial_\mu\partial_\mu\partial_\mu K(\mathbf{R}_0)}{K(\mathbf{R}_0)^2}\right]\\&\quad=\exp\left\{-\frac{6D\tau_D}{R_0^2}\frac{5(R_0/R_F)^{-6}}{[1+(R_0/R_F)^{-6}]^2}\right\},\end{aligned} \tag{40}$$

where τ_D is the fluorescence lifetime of the donor dye without acceptor. When the diffusion coefficient increases, small R_0 or large FRET rate will be favored, thus the lifetime distribution will be shifted toward small τ, hence the ensemble averaged lifetime decreases. Variational treatment by Portman and Wolynes has rigorously proved that the static and the dynamic averages are the upper and the lower bounds on the ensemble averaged survival probability for general diffusion-controlled reactions.[44] In the limit when $D\to 0$, the small FRET rate contribution will be maximized and the lifetime reduces to the reaction time for a static configuration, $\tau = K^{-1}$. Given the functional form of the energy transfer rate, each measurement of lifetime corresponds to a fixed donor–acceptor distance. Therefore, by measuring the FRET lifetime distribution, one can map out the distribution function of interfluorophore distance. This mapping however is modified according to Eq. (40) by taking into account the diffusional effect.

VI. INTRINSIC VISCOSITY

From standard viscoelasticity theory, the stress tensor is measured under the external shear flow $v_x = \alpha(t)y$ and is related to the desired time-dependent viscoelasticity $\eta(t)$ through $\sigma_{xy}(t) = \eta_s + \int_\infty^t \eta_p(t-t')\alpha(t')$, where $\eta_p(t)$ is the viscosity contribution from polymers. Given $\eta(t)$, the intrinsic viscosity is $[\eta] = \int_0^\infty \eta_p(\tau)d\tau/(\rho\eta_s)$, where ρ is the mass density of the polymer and η_s is the solvent viscosity. Similarly, we can determine the storage modulus $G'(\omega)$ and the loss modulus $G''(\omega)$ from the viscoelastic response $\eta_p(t)$.

We derive the microscopic expression for the polymer viscosity $\eta_p(t)$. We begin with the definition of the intrinsic stress tensor

$$\langle \sigma_{p,xy}(t)\rangle = -\frac{c}{N}\sum_n \int F_{nx} r_{ny} P d^N\mathbf{r}, \tag{41}$$

where P is the distribution function of the Gaussian chain at time t and c is the number concentration of the beads. In Eq. (41), the solvent contribution is not included in the stress and $\sigma_{p,xy}(t)$ is the contribution from single polymers. Under the shear flow, the distribution function of the polymer chain follows $\dot{P}(t) = \mathcal{L}P(t) - \Sigma_m \partial_{mx}[\alpha(t) r_{my} P(t)]$ where the operator $\mathcal{L}$ dictates the free propagation of the polymer and the second term is due to the external flow. To first order in perturbation, we have

$$P(t) = P_0 - \int_{-\infty}^{t} e^{\mathcal{L}(t-\tau)} \sum_m \frac{\partial}{\partial r_{mx}} \alpha(\tau) r_{my} P_0(\tau) d\tau, \tag{42}$$

where $P_0 = P_{\mathrm{eq}}$ is the equilibrium distribution. Substituting Eq. (42) into Eq. (41), we find

$$\eta_p(t) = \frac{c}{N}\beta \left\langle \sum_n F_{nx}(t) r_{ny}(t) \sum_n r_{mx}(0) F_{my}(0) \right\rangle, \tag{43}$$

which is the linear response expression found in literature.[36,38,46,47] Applying the Gaussian factorization to the above-given expression leads to

$$\eta_p(t) \approx \frac{c}{N}\beta \sum_{nm} \langle F_{nx}(t) r_{mx}(0)\rangle \langle F_{my}(0) r_{ny}(t)\rangle$$

$$= \sum_{nm} \frac{c}{N} k_B T \left\langle \frac{\partial r_{mx}(t)}{\partial r_{nx}(0)} \right\rangle \left\langle \frac{\partial r_{ny}(t)}{\partial r_{my}(0)} \right\rangle, \tag{44}$$

where we assume the motions along different Cartesian coordinates are decoupled. The Gaussian factorization and the decoupling assumption hold exactly for the Brownian motion of Gaussian chains.

The key result of this section is the last expression in Eq. (44), which relates single chain measurements to macroscopic viscoelastic responses. Here, the stability function $\partial \mathbf{r}_{mx}/\partial \mathbf{r}_{nx}$ measures the divergence of the trajectories with respect to initial conditions and cannot be obtained directly from bulk measurements. By virtue of this expression, we can evaluate the intrinsic viscoelasticity of a Gaussian chain by tracking bead motions along a polymer chain.

Accurate evaluation of the exact expression in Eq. (43) has been carried out by Pyun and Fixman, Bixon and Zwanzig, etc.[35–37] We will calculate the viscosity within the semiflexible Gaussian model. The viscoelasticity function in Eq. (44) can be transformed into normal modes as

$$\frac{\partial \mathbf{r}_{mx}(t)}{\partial \mathbf{r}_{nx}} = \sum_p^{N-1} \frac{\partial \mathbf{r}_{mx}(t)}{\partial \mathbf{x}_{px}(t)} \exp\left[-\frac{\lambda_p}{\zeta_p} t\right] \frac{\partial \mathbf{x}_{px}}{\partial \mathbf{r}_{nx}}, \tag{45}$$

where $\partial \mathbf{r}_{mx}/\partial \mathbf{x}_{px}$ is the unitary transform matrix element between the real coordinates and normal modes. For the semiflexible Gaussian chain, $\eta_p(t)$ can be written as a sum over the exponentially decaying correlation functions of the normal modes

$$\eta_p(t) = k_B T \frac{c}{N} \sum_{p=1}^{N-1} \exp\left[-\frac{t}{\tau_p}\right], \tag{46}$$

where $\tau_p = \xi_p/(2\lambda_p)$ is the decay time for each normal mode. In general, application of a shear flow does not invoke stretching modes, thus, only the bending motion of the polymer chain is considered in the expression for $\eta_p(t)$. Therefore the intrinsic storage modulus and the intrinsic loss modulus are $[G'(\omega)]_p = \int_0^\infty \omega \sin \omega t \, \Sigma_{p=1}^{N-1} \exp[-t/\tau_p] dt$ and $[G''(\omega)]_p = \Sigma_0^\infty \omega \cos \omega t \, \Sigma_{p=1}^{N-1} \exp[-t/\tau_p]$. Given the expression for λ_p in Eq. (A2) and $\zeta_p = 2N\zeta$, we have

$$\tau_p = \begin{cases} \dfrac{N^2 a_0^2 \zeta L_p}{3\pi^2 k_b T} p^{-2} = \tau_1 p^{-2}, & L_p \ll N \\ \dfrac{N^4 a_0^2 \zeta}{3\pi^4 k_B T L_p} p^{-4} = \tau_1' p^{-4}, & L_p \geqslant N, \end{cases} \tag{47}$$

which describes both the flexible chain when $L_p \ll N$ and the stiff rod when $L_p \geqslant N$. In the limit $L_p = 1/2$, the above-given expression recovers the time constants for pth normal mode of the Rouse chain.[29] The expressions for $[G'(\omega)]_p$ and $[G''(\omega)]_p$ simplify in the following two cases:

(1) In the low frequency limit, $\omega\tau_1 \ll 1$ and $\omega\tau_1' \ll 1$ $[G'(\omega)]_p$ and $[G''(\omega)]_p$ are approximated as

$$[G'(\omega)]_p \approx \begin{cases} (\omega\tau_1)^2 \Sigma_{p=1}^\infty p^{-4} = \pi^4 (\omega\tau_1)^2/90, & L_p \ll N \\ (\omega\tau_1')^2 \Sigma_{p=1}^\infty p^{-8} = \pi^8 (\omega\tau_1')^2/9450, & L_p \geqslant N, \end{cases} \tag{48}$$

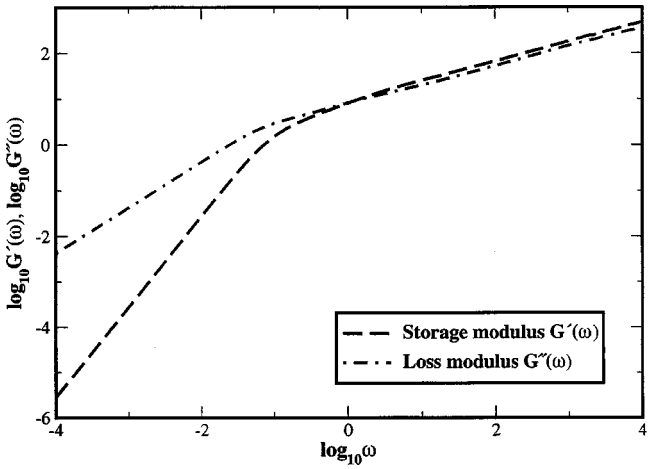

FIG. 6. The intrinsic and loss storage modulus for a flexible chain with 5000 beads and the persistence length taken as 5. At low frequencies, $G'(\omega)$ scales as ω^2 and $G''(\omega)$ scales as ω. At high frequencies, both $G'(\omega)$ and $G''(\omega)$ scale as $\omega^{1/2}$.

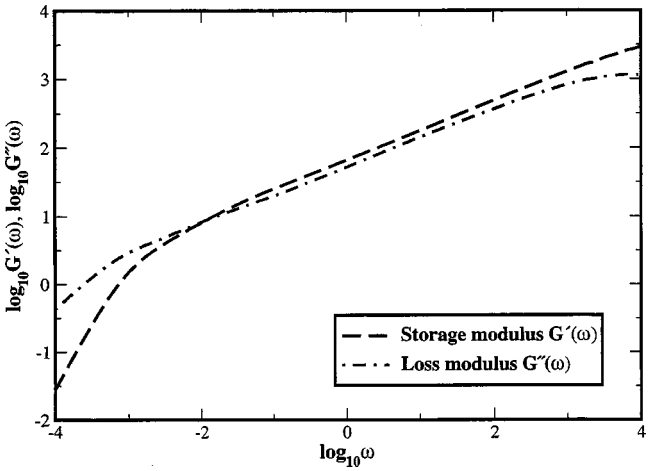

FIG. 7. The intrinsic and loss storage modulus for a semiflexible chain with 5000 beads and the persistence length taken as 500. At low frequencies, $G'(\omega)$ and $G''(\omega)$ scales as ω^2 and ω, respectively. At high frequencies, both $G'(\omega)$ and $G''(\omega)$ scales as $\omega^{1/4}$.

and

$$[G''(\omega)]_p \approx \begin{cases} \omega\tau_1 \Sigma_{p=1}^{\infty} p^{-2} = \pi^2 \omega\tau_1/6, & L_p \ll N \\ \omega\tau_1' \Sigma_{p=1}^{\infty} p^{-4} = \pi^4 \omega\tau_1'/90, & L_p \gg N. \end{cases} \quad (49)$$

Therefore, $[G'(\omega)]_p$ and $[G''(\omega)]_p$ are proportional to ω^2 and ω, respectively, and reduce to the stiff rod limit when $L_p \gg N$.

(2) In the high frequency limit, $\omega\tau_1 \gg 1$ and $\omega\tau_1' \gg 1$, the sum over p is approximated by an integral, so that

$$[G'(\omega)]_p \approx \begin{cases} (\omega\tau_1)^{1/2}\pi/[4\sin(\pi/4)], & L_p \ll N \\ (\omega\tau_1')^{1/4}\pi/[8\sin(\pi/8)], & L_p \gg N \end{cases} \quad (50)$$

and

$$[G''(\omega)]_p \approx \begin{cases} (\omega\tau_1)^{1/2}\pi/[4\cos(\pi/4)], & L_p \ll N \\ (\omega\tau_1')^{1/4}\pi/[8\cos(\pi/8)], & L_p \gg N. \end{cases} \quad (51)$$

For the stiff chain, the bending motion has a $\omega^{1/4}$ dependence at high frequency, which implies $\eta_p(t) \propto t^{-1/4}$ when $t \ll \tau_1'$. This is consistent with the findings of the polymer bending motion in Refs. 48 and 49.

As shown in Figs. 6 and 7, numerical calculations of the intrinsic storage $G'(\omega)$ and loss moduli $G''(\omega)$ from the viscoelastic response function $\eta_p(t)$ in Eq. (46) confirm the two different scaling regions for both flexible and semiflexible chains. In the numerical calculation, the number of beads on the polymer chain is taken as 5000, the persistence length L_p is 5 for the flexible chain and 500 for a semiflexible chain.

In θ solvent, the intrinsic moduli for the semiflexible chain can be calculated with τ_p obtained by the preaveraging method in standard textbook,[29] as shown in Appendix D.

(1) In the low frequency limit, similar to the above-mentioned derivation, $[G'(\omega)]_p$ and $[G''(\omega)]_p$ are still proportional to ω^2 and ω, respectively.

(2) In the high frequency limit,

$$[G'(\omega)]_p \approx \begin{cases} (\omega\tau_1)^{2/3}\pi/[3\sin(\pi/3)], & L_p \ll N \\ (\omega\tau_1')^{2/7}\pi/[7\sin(\pi/7)], & L_p \gg N \end{cases} \quad (52)$$

and

$$[G''(\omega)]_p \approx \begin{cases} (\omega\tau_1)^{2/3}\pi/[3\cos(\pi/3)], & L_p \ll N \\ (\omega\tau_1')^{2/7}\pi/[7\cos(\pi/7)], & L_p \gg N, \end{cases} \quad (53)$$

which are proportional to $\omega^{2/3}$ and $\omega^{2/7}$, respectively.

VII. CONCLUDING REMARKS

In Secs. II and III, we formulated the semiflexible Gaussian chain with analog to the Ornstein–Uhlenbeck random walk process and incorporated the persistent length into the Rouse model. The mean square bead–bead distance $\langle \mathbf{R}_{nm}^2 \rangle$ is studied for different degrees of stiffness. For a flexible chain, the mean square distance exhibits the scaling relation for a random Gaussian coil $\langle \mathbf{R}_{nm}^2 \rangle = 2L_p|n-m|a_0^2$; while for large persistence length, it scales as a rigid rod, $\langle \mathbf{R}_{nm}^2 \rangle = |n-m|^2 a_0^2$. To study the intrachain motion of semiflexible chains, the evolution of $\mathbf{R}_{nm}$ is calculated based on the normal mode decomposition of the Langevin equation of a semiflexible polymer chain. The resulting Green's function resembles a Gaussian process within a potential of mean force. The Brownian dynamics of the semiflexible chain shows that the correlation function $\langle \mathbf{R}_{nm}(t) \cdot \mathbf{R}_{nm}(0) \rangle$ has a much longer time scale for a stiff chain than for a flexible polymer.

In Sec. IV, we have considered the fluorescence resonant energy transfer (FRET) process on a semiflexible chain, where a donor–acceptor pair attached to the nth and the mth polymer beads are used to probe the conformational dynamics. The fluorescence lifetime correlation function and the FRET efficiency correlation function are closely related to the normalized distance correlation function $\phi(t)$. Thus both the lifetime correlation and the FRET efficiency correlation can be employed as possible measures of the intrachain dynamics. Furthermore, the instantaneous diffusion coefficient due to finite time resolution t_{bin} has been calculated within

the theoretical model. As $t_{\rm bin}\to 0$, the instantaneous diffusion coefficient is obtained from the independent diffusive motion of the donor and acceptor sites. When measured with finite time resolution, the instantaneous diffusion coefficient $\overline{D}(R_{nm}^2)=\langle R_{nm}^2\rangle[1-\phi^2(t_{\rm bin})]/t_{\rm bin}+R_{nm}^2[1-\phi(t_{\rm bin})]^2/t_{\rm bin}$ is much smaller in the collapsed structure than in the ordered structure, and the variation has a quadratic dependence on the donor–acceptor distance R_{nm}. Some of these predictions are in qualitative agreement with reported experiments.[11]

In FRET experiments, the intrachain dynamics usually occurs on a much longer time scale than the energy transfer reaction. In Sec. V, the FRET lifetime is discussed in the fast reaction limit. With inhomogeneous cumulant expansion, we have shown that the lifetime is a weighted reaction time for a given initial configuration, $\tau=K(\mathbf{R}_0)^{-1}\times\exp[-D\Sigma_\mu\partial_\mu\partial_\mu K(\mathbf{R}_0)/K(\mathbf{R}_0)^2]$. When the intrachain relaxation process is extremely slow, $D\to 0$, this expression recovers the static limit, i.e., $\tau=K^{-1}$, and thus, the distribution function of the donor–acceptor distance can be mapped out from the single-molecule lifetime measurements. Furthermore, recent measurements of the viscosity-dependent intramolecular quenching rate provide detailed information from the reaction-controlled limit to the diffusion-controlled limit.[33,34,50] Thus systematic studies and detailed analysis of the ensemble averaged lifetime is necessary to better understand the polymer dynamics.[51]

The macroscopic viscoelastic response of a polymer chain is related to the bead dynamics on a single polymer by Eq. (44), from which the intrinsic elastic moduli are derived. Explicit evaluations of the elastic storage modulus and the elastic loss modulus are performed with the consideration of the persistence length L_p. Our expressions exactly recover the results for the Rouse chain in the limit $L_p\to 1/2$, and predict the correct scaling over frequency for the bending motion of a stiff polymer in the stiff rod limit $L_p\geqslant N$.

Single-molecule FRET measurements of the semiflexible chain yield rich information about intrachain motion, for example, mean square distance, distance correlation function, instantaneous diffusion coefficient, and intrinsic viscosity. Further refinements of single-molecule spectroscopy will provide more accurate methods to examine the details of the intra-polymer interactions and lead to better understanding of the related issues such as protein folding and self-assembly of biological systems. Further consideration of hydrodynamic and excluded volume effects can be implemented in the theoretical model for a semiflexible chain.

ACKNOWLEDGMENT

This research is supported by the NSF Career Award.

APPENDIX A: APPROXIMATE NORMAL MODES OF SEMIFLEXIBLE CHAINS

In a semiflexible chain, the potential energy is

$$U=\frac{3k_BT}{8a_0^2}\sum_{n=1}^{N-2}\left[\frac{1+b}{1-b}(\mathbf{u}_{n+1}-\mathbf{u}_n)^2+\frac{1-b}{1+b}(\mathbf{u}_{n+1}+\mathbf{u}_n)^2\right]+\frac{3k_BT}{4a_0^2}(\mathbf{u}_1^2+\mathbf{u}_{N-1}^2), \tag{A1}$$

where $\mathbf{u}_n=\mathbf{R}_{n+1}-\mathbf{R}_n$ is the bond between the nth and the $n+1$th beads. In the continuous limit, the potential energy reduces to Eq. (5) in Sec. II. Applying the transform of Eq. (7), we can decompose the potential energy into three parts $U=T_1+T_2+T_3$, where

$$T_1=\frac{3k_BT}{8a_0^2}\frac{1+b}{1-b}\sum_{n=1}^{N-2}(\mathbf{u}_{n+1}-\mathbf{u}_n)^2=\frac{12Nk_BT}{a_0^2}\sum_{p=1}^{N-1}\mathbf{x}_p^2\frac{1+b}{1-b}\sin^4\frac{p\pi}{2N}-\frac{1+b}{1-b}\cdot T_3,$$

$$T_2=\frac{3k_BT}{8a_0^2}\frac{1-b}{1+b}\sum_{n=1}^{N-2}(\mathbf{u}_{n+1}+\mathbf{u}_n)^2=\frac{12Nk_BT}{a_0^2}\sum_{p=1}^{N-1}\mathbf{x}_p^2\frac{1-b}{1+b}\sin^2\frac{p\pi}{2N}\cos^2\frac{p\pi}{2N}-\frac{1-b}{1+b}\cdot T_3,$$

$$T_3=\frac{3k_BT}{4a_0^2}(\mathbf{u}_1^2+\mathbf{u}_{N-1}^2)=\frac{24k_BT}{a_0^2}\sum_{p,q=1}^{N-1}\mathbf{x}_p\cdot\mathbf{x}_q\sin^2\frac{p\pi}{2N}\sin^2\frac{q\pi}{2N}\times[(-1)^{p+q}+1]\cos\frac{p\pi}{2N}\cos\frac{q\pi}{2N}.$$

Therefore, in the large N limit, the off-diagonal terms are N times smaller than the diagonal terms, and we approximately diagonalize the potential energy in normal modes, $U\approx\sum_{p=1}^{N-1}\lambda_p\mathbf{x}_p^2/2$ with

$$\lambda_p=\frac{24Nk_BT}{a_0^2}\sin^2\frac{p\pi}{2N}\left(2L_p\sin^2\frac{p\pi}{2N}+\frac{1}{2L_p}\cos^2\frac{p\pi}{2N}\right), \tag{A2}$$

where $2L_p=(1+b)/(1-b)$ is the persistent length. In the limit of the flexible chain, the persistent length is relatively small compared to the contour length of the chain, the second term dominates and yields

$$\lambda_p\approx\frac{24Nk_BT}{a_0^2}\sin^2\frac{p\pi}{2N}\frac{1}{2L_p}\cos^2\frac{p\pi}{2N}\approx\frac{3\pi^2k_BT}{Na_0^2L_p}p^2. \tag{A3}$$

In the limit of $L_p\to 1/2$ or $b\to 0$, λ_p given in Eq. (A2) is exactly the same as the result for Rouse chain.[29] In the strong persistence limit, the first term also contributes and may even dominate for large p, yielding the worm-like chain normal modes,

$$\lambda_p\approx\frac{3\pi^2k_BTp^2}{Na_0^2L_p}\left(1+\frac{\pi^2L_p^2}{N^2}p^2\right)\approx\frac{3k_BT\pi^4L_p}{N^3a_0^2}p^4. \tag{A4}$$

In this expression, all the normal modes will be suppressed for a rigid-rod-like chain for $L_p \to \infty$ while keeping only the center of mass motion, which is a deficit of the approximate normal modes we obtained in this section. Full motion of the chain can be observed from numerical solutions of the original equation of motion in Eq. (6).

APPENDIX B: GREEN'S FUNCTION FOR THE SEMIFLEXIBLE GAUSSIAN CHAIN

As demonstrated in Appendix A, the potential energy of a semiflexible Gaussian chain is approximately diagonal and quadratic in normal coordinates $\mathbf{x}_p$ as shown in Appendix A. The evolution of the normal modes follows the Smoluchowski equation,

$$\frac{\partial P}{\partial t} = \mathcal{L} P(t),$$

with

$$\mathcal{L} = \sum_{p=1}^{N-1} \frac{1}{\zeta_p} \frac{\partial}{\partial \mathbf{x}_p} \left(k_B T \frac{\partial}{\partial \mathbf{x}_p} + \lambda_p \mathbf{x}_p \right). \tag{B1}$$

Solution of the above-given Fokker–Planck equation gives the Green's function

$$G(\mathbf{x}_p, t | \mathbf{x}_p(0)) = \prod_{p=1}^{N-1} \left[\frac{2\pi k_B T}{\lambda_p} \left(1 - \exp\left(-2 \frac{\lambda_p}{\zeta_p} t \right) \right) \right]^{-3/2} \times \exp\left\{ - \frac{\sum_{p=1}^{N-1} \lambda_p \left[\mathbf{x}_p - \mathbf{x}_p(0) \exp\left(-\frac{\lambda_p}{\zeta_p} t \right) \right]^2}{2 k_B T \left(1 - \exp\left(-2 \frac{\lambda_p}{\zeta_p} t \right) \right)} \right\}, \tag{B2}$$

and the equilibrium distribution of normal modes

$$P_{\mathrm{eq}}(\mathbf{x}_p) = \prod_{p=1}^{N-1} \left(\frac{2\pi k_B T}{\lambda_p} \right)^{-3/2} \exp\left\{ - \frac{\sum_{p=1}^{N-1} \lambda_p \mathbf{x}_p^2}{2 k_B T} \right\}. \tag{B3}$$

The correlation function of the pth normal mode is calculated directly from above as $\langle \mathbf{x}_p(t) \cdot \mathbf{x}_p(0) \rangle = 3 k_B T / \lambda_p \times \exp[-\lambda_p t / \zeta_p]$, and the equilibrium average of $\mathbf{R}_{nm}$ and the correlation between $\mathbf{R}_{nm}(0)$ and $\mathbf{R}_{nm}(t)$ can be evaluated according to the decomposition in Eq. (12),

$$\langle \mathbf{R}_{nm}^2 \rangle = \sum_{p=1}^{N-1} (c_{nm}^p)^2 \frac{3 k_B T}{\lambda_p}, \tag{B4}$$

$$\phi(t) = \frac{\langle \mathbf{R}_{nm}(t) \cdot \mathbf{R}_{nm}(0) \rangle}{\langle \mathbf{R}_{nm}^2 \rangle} = [\langle \mathbf{R}_{nm}^2 \rangle]^{-1} \sum_{p=1}^{N-1} (c_{nm}^p)^2 \frac{3 k_B T}{\lambda_p} \exp\left[-\frac{\lambda_p}{\zeta_p} t \right]. \tag{B5}$$

$\mathbf{R}_{nm}$ is a Gaussian variable because it is a linear combination of Gaussian normal modes. The equilibrium distribution of $\mathbf{R}_{nm}$ is

$$P_{\mathrm{eq}}(\mathbf{R}_{nm}) = \int d\mathbf{x}_p \, \delta\left(\mathbf{R}_{nm} - \sum_{p=1}^{N-1} c_{nm}^p \mathbf{x}_p \right) P_{\mathrm{eq}}(\mathbf{x}_p) = \left[\frac{2\pi}{3} \langle \mathbf{R}_{nm}^2 \rangle \right]^{-3/2} \exp\left\{ - \frac{3 \mathbf{R}_{nm}^2}{2 \langle \mathbf{R}_{nm}^2 \rangle} \right\}, \tag{B6}$$

where cumulant expansion over the Gaussian normal modes and Eq. (B4) are applied. In a similar fashion it can be shown that the joint distribution for $\mathbf{R}_{nm}(t)$ and $\mathbf{R}_{nm}(0)$ is

$$P(\mathbf{R}_{nm}(t), t, \mathbf{R}_{nm}(0)) = \left[\frac{4\pi^2}{9} \langle \mathbf{R}_{nm}^2 \rangle^2 (1 - \phi(t)^2) \right]^{-3/2} \times \exp\left\{ - \frac{3[\mathbf{R}_{nm}^2(t) - 2\phi(t) \mathbf{R}_{nm}(t) \cdot \mathbf{R}_{nm}(0) + \mathbf{R}_{nm}^2(0)]}{2 \langle \mathbf{R}_{nm}^2 \rangle (1 - \phi(t)^2)} \right\}, \tag{B7}$$

and the evolution of $\mathbf{R}_{nm}$ is described by the corresponding Green's function,

$$G(\mathbf{R}_{nm}(t), t | \mathbf{R}_{nm}(0)) = \frac{P(\mathbf{R}_{nm}(t), t, \mathbf{R}_{nm}(0))}{P_{\mathrm{eq}}(\mathbf{R}_{nm}(0))} = \left[\frac{2\pi}{3} \langle \mathbf{R}_{nm}^2 \rangle (1 - \phi(t)^2) \right]^{-3/2} \times \exp\left\{ - \frac{3(\mathbf{R}_{nm}(t) - \phi(t) \mathbf{R}_{nm}(0))^2}{2 \langle \mathbf{R}_{nm}^2 \rangle (1 - \phi(t)^2)} \right\}. \tag{B8}$$

APPENDIX C: FRET RATE DISTRIBUTION AND CORRELATION OF SEMIFLEXIBLE GAUSSIAN CHAIN

The FRET rate depends on the distance R between the donor and the acceptor as $K(R) = k_F (R_F / R)^6$, where R_F is the Förster radius at which the transfer efficiency is 50%, and k_F is the energy transfer rate at $R = R_F$. However, this rate expression diverges at $R \to 0$ where the transition dipole–dipole interaction no longer holds. To facilitate the calculation, we choose a slightly modified expression of $K(R)$ as

$$K(R) = \frac{k_F}{\epsilon + (R/R_F)^6}, \tag{C1}$$

where ϵ is a small quantity that denotes the breakdown of the weak dipole–dipole interaction when R is extremely small. It is shown later in this section that the average transfer rate $\langle K(R) \rangle$ is a large quantity because ϵ is usually small. The overall decay rate of the fluorescence on the donor molecule can be approximated by neglecting the radiative decay. The three-dimensional Fourier transform of the rate function $K(R)$ is

$$K(\mathbf{q}) = \frac{2\pi^2 k_F R_F^2}{3 q \epsilon^{2/3}} \left\{ \exp[-q R_F \epsilon^{1/6}] + \exp\left[-\frac{q R_F \epsilon^{1/6}}{2} \right] \cdot \left[-\cos\left(\frac{\sqrt{3}}{2} q R_F \epsilon^{1/6} \right) + \sqrt{3} \sin\left(\frac{\sqrt{3}}{2} q R_F \epsilon^{1/6} \right) \right] \right\}. \tag{C2}$$

Considering ϵ is a small number and $qR_F\epsilon^{1/6} \ll 1$, the leading order of $K(\mathbf{q})$ is

$$K(\mathbf{q}) \approx \frac{2\pi^2 R_F^3 k_F}{3\sqrt{\epsilon}}, \tag{C3}$$

which approximates energy transfer by a delta-function sink. Because $\mathbf{R}_{nm}$ is a Gaussian variable with distribution Eq. (B6), the cumulant expansion yields $\langle \exp[i\mathbf{q}\cdot\mathbf{R}_{nm}]\rangle = \exp[-q^2\langle \mathbf{R}_{nm}^2\rangle/6]$, and the average over $K(\mathbf{R}_{nm})$ and the correlation of $K(\mathbf{R}_{nm})$ are evaluated as

$$\begin{aligned}\langle K(\mathbf{R}_{nm})\rangle &= \int_{\mathbf{q}} K(\mathbf{q}) \exp[-q^2\langle \mathbf{R}_{nm}^2\rangle/6] \\ &= k_F \sqrt{\frac{3\pi}{2\epsilon}} \left(\frac{\langle \mathbf{R}_{nm}^2\rangle}{R_F^2}\right)^{-3/2},\end{aligned} \tag{C4}$$

$$\begin{aligned}&\langle K(\mathbf{R}_{nm}(t)) G(t) K(\mathbf{R}_{nm}(0))\rangle \\ &= \int_{\mathbf{q}}\int_{\mathbf{q}'} K(\mathbf{q}) K(\mathbf{q}') \exp\left\{-\frac{\langle \mathbf{R}_{nm}^2\rangle}{6}[q^2 + q'^2 \right. \\ &\left. + 2\mathbf{q}\cdot\mathbf{q}'\phi(t)]\right\} \approx k_F^2 \frac{3\pi}{2\epsilon}\left(\frac{\langle \mathbf{R}_{nm}^2\rangle}{R_F^2}\right)^{-3} [1-\phi^2(t)]^{-3/2},\end{aligned} \tag{C5}$$

where $\int_{\mathbf{q}}$ stands for $\int d^3q/(2\pi)^3$ and $\phi(t) = \langle \mathbf{R}_{nm}(t)\cdot\mathbf{R}_{nm}(0)\rangle / \langle \mathbf{R}_{nm}^2\rangle$. Therefore the memory function $\chi(t)$ is directly related to the distance correlation function $\phi(t)$ as

$$\begin{aligned}\chi(t) &= \frac{\langle K(\mathbf{R}_{nm}(t)) G(t) K(\mathbf{R}_{nm}(0))\rangle}{\langle K(\mathbf{R}_{nm})\rangle^2} - 1 \\ &= [1-\phi^2(t)]^{-3/2} - 1 = \sum_{l=1}^{\infty} (2l+1)!!/(2^l l!)\phi^{2l}(t),\end{aligned} \tag{C6}$$

where $(2l+1)!! = (2l+1)\cdot(2l-1)\cdots 3\cdot 1$. If we are able to calculate the correlation function $\phi(t)$, the corresponding correlation function for FRET rates is determined accordingly.

APPENDIX D: HYDRODYNAMIC INTERACTIONS IN SEMIFLEXIBLE GAUSSIAN CHAINS

In θ solvent, the hydrodynamic interactions among polymer beads must be considered. With the preaveraging technique introduced in the Zimm model,[29] we are able to evaluate the normal modes of semiflexible chain approximately.

In the long chain limit when $L_p \ll N$, the persistent length introduces slight deviations from the Zimm model in θ solvent, and we have

$$\zeta_p = (2L_p)^{1/2}\zeta_p^{\mathrm{ZM}}, \tag{D1}$$

$$\lambda_p = \frac{1}{2L_p}\lambda_p^{\mathrm{ZM}}, \tag{D2}$$

$$\tau_p = \frac{\zeta_p}{\lambda_p} = (2L_p)^{3/2}\tau_p^{\mathrm{ZM}}, \tag{D3}$$

where the superscript "ZM" means the corresponding quantities in the Zimm model,

$$\zeta_P^{\mathrm{ZM}} = \eta_s (12\pi^3 N a_0^2 p)^{1/2}, \tag{D4}$$

$$\lambda_p^{\mathrm{ZM}} = \frac{6\pi^2 k_B T}{N a_0^2} p^2, \tag{D5}$$

$$\tau_p^{\mathrm{ZM}} = \tau_1^{\mathrm{ZM}} p^{-3/2}. \tag{D6}$$

It is obvious that all the above-given relations reduce to the Rouse model when $L_p = 1/2$.

In the short chain limit when $L_p \gg N$, the corresponding quantities are

$$\zeta_p \approx (12\pi^3)^{1/2}\eta_s a_0 p^{1/2} N^{1/2}, \tag{D7}$$

$$\lambda_p \approx \frac{3\pi^4 k_B T L_p}{N^3 a_0^2} p^4, \tag{D8}$$

$$\tau_p = \tau_1 p^{-7/2}. \tag{D9}$$

[1] T. Bache, W. E. Moerner, M. Orrit, and U. P. Wild, *Single Molecule Optical Detection, Imaging and Spectroscopy* (VCH, Berlin, 1996).
[2] X. S. Xie and J. K. Trautman, Annu. Rev. Phys. Chem. **49**, 441 (1998).
[3] L. Edman, U. Mets, and R. Rigler, Proc. Natl. Acad. Sci. U.S.A. **93**, 6710 (1996).
[4] Y. Jia, A. Sytnik, L. Li, S. Vladimirov, B. S. Cooperman, and R. M. Hochstrasser, Proc. Natl. Acad. Sci. U.S.A. **94**, 7932 (1997).
[5] E. Geva and J. L. Skinner, Chem. Phys. Lett. **288**, 225 (1998).
[6] J. Wang and P. G. Wolynes, Phys. Rev. Lett. **74**, 4317 (1995).
[7] A. M. Berezhkovskii, A. Szabo, and G. H. Weiss, J. Chem. Phys. **110**, 9145 (1999).
[8] S. Weiss, Science **283**, 1676 (1999).
[9] T. Ha, A. Y. Ting, J. Liang, W. B. Caldwell, A. A. Deniz, D. S. Chemla, P. G. Schultz, and S. Weiss, Proc. Natl. Acad. Sci. U.S.A. **96**, 893 (1999).
[10] A. A. Deniz, T. A. Laurence, G. S. Beligere, M. Dahan, A. B. Martin, D. S. Chemla, P. E. Dawson, P. G. Schultz, and S. Weiss, Proc. Natl. Acad. Sci. U.S.A. **97**, 5179 (2000).
[11] D. S. Talaga, W. L. Lau, H. Roder, J. Tang, Y. Jia, W. F. DeGrado, and R. M. Hochstrasser, Proc. Natl. Acad. Sci. U.S.A. **97**, 13021 (2000).
[12] M. Lee, J. Tang, and R. M. Hochstrasser, Chem. Phys. Lett. **344**, 501 (2001).
[13] L. Stryer, Annu. Rev. Biochem. **47**, 819 (1978).
[14] A. Hillisch, M. Lorenz, and S. Diekmann, Curr. Opin. Struct. Biol. **11**, 201 (2001).
[15] C. Eggeling, J. Wildengren, R. Rigler, and C. A. M. Seidel, Anal. Chem. **70**, 2651 (1998).
[16] D. E. Smith and S. Chu, Science **281**, 1335 (1998).
[17] S. R. Quake, H. P. Babcock, and S. Chu, Nature (London) **388**, 151 (1997).
[18] D. E. Smith, H. P. Babcock, and S. Chu, Science **283**, 1724 (1999).
[19] O. Kratky and G. Porod, Recl. Trav. Chim. Pays-Bas. **68**, 1106 (1949).
[20] G. Porod, J. Polym. Sci. **10**, 157 (1953).
[21] R. A. Harris and J. E. Hearst, J. Chem. Phys. **44**, 2595 (1966).
[22] J. E. Hearst, R. A. Harris, and E. Beals, J. Chem. Phys. **45**, 3106 (1966).
[23] J. E. Hearst and R. A. Harris, J. Chem. Phys. **46**, 298 (1967).
[24] K. F. Freed, J. Chem. Phys. **54**, 1453 (1971).
[25] K. F. Freed, Adv. Chem. Phys. **22**, 1 (1972).
[26] M. Fixman and J. Kovac, J. Chem. Phys. **58**, 1564 (1973).
[27] B.-Y. Ha and D. Thirumalai, J. Chem. Phys. **106**, 4243 (1997).
[28] B. H. Zimm, J. Chem. Phys. **24**, 269 (1956).
[29] M. Doi and S. F. Edwards, *The Theory of Polymer Dynamics* (Oxford University Press, New York, 1986).
[30] T. G. Mason and D. A. Weitz, Phys. Rev. Lett. **74**, 1250 (1995).
[31] J. C. Crocker, M. T. Valentine, E. R. Weeks, T. Gisler, P. D. Kaplan, A. G. Yodh, and D. A. Weitz, Phys. Rev. Lett. **85**, 888 (2000).
[32] J. G. Kirkwood, Recl. Trav. Chim. Pays-Bas. **68**, 649 (1949).
[33] O. Bieri, J. Wirz, B. Hellrung, M. Schutkowski, M. Drewello, and T. Kiefhaber, Proc. Natl. Acad. Sci. U.S.A. **96**, 9597 (1999).
[34] L. J. Lapidus, W. A. Eaton, and J. Hofrichter, Proc. Natl. Acad. Sci. U.S.A. **97**, 7220 (2000).

[35] C. W. Pyun and M. Fixman, J. Chem. Phys. **44**, 2107 (1966).
[36] M. Bixon, J. Chem. Phys. **58**, 1459 (1973).
[37] M. Bixon and R. Zwanzig, J. Chem. Phys. **68**, 1890 (1978).
[38] B. U. Felderhof, J. M. Deutch, and U. M. Titulaer, J. Chem. Phys. **63**, 740 (1975).
[39] R. G. Winkler, P. Reineker, and L. Harnau, J. Chem. Phys. **101**, 8119 (1994).
[40] J. B. Lagowski, J. Noolandi, and B. Nickel, J. Chem. Phys. **95**, 1266 (1991).
[41] R. G. Winkler, Phys. Rev. Lett. **82**, 1843 (1999).
[42] R. W. Pastor, R. Zwanzig, and A. Szabo, J. Chem. Phys. **105**, 3878 (1996).
[43] G. Srinivas and B. Bagchi, J. Chem. Phys. **116**, 837 (2002).
[44] J. J. Portman and P. G. Wolynes, J. Phys. Chem. A **103**, 10602 (1999).
[45] G. Diezemann, J. Chem. Phys. **116**, 1647 (2002).
[46] H. Yamakawa, G. Tanaka, and W. H. Stockmayer, J. Chem. Phys. **61**, 4535 (1974).
[47] W. H. Stockmayer, G. Wilemski, H. Yamakawa, and G. Tanaka, J. Chem. Phys. **63**, 1039 (1975).
[48] M. Pasquali, V. Shankar, and D. C. Morse, Phys. Rev. E **64**, 020802 (2001).
[49] F. Gittes and F. C. Mackintosh, Phys. Rev. E **58**, R1241 (1998).
[50] L. J. Lapidus, P. J. Steinbach, W. A. Eaton, A. Szabo, and J. Hofrichter, J. Phys. Chem. (submitted).
[51] S. Yang and J. Cao, J. Chem. Phys. **117**, 10996 (2002), preceding paper.